The RELEVANCE OF HANLE EFFECT ON NA AND FE LIDARS

Chiao-Yao (Joe) She[1*]

[1]*Physics Department, Colorado State University, Fort Collins, CO, 80523 U.S.A.*
**Email: joeshe@colostate.edu*

ABSTRACT

A laser resonant scattering process involves two steps, excitation and emission. That emission occurs spontaneously is well accepted. That the atoms involved in the emission are excited coherently by a laser beam leading to a non-isotropic angular distribution of emission (an antenna pattern) is not well known. The difference between coherent and incoherent excitation leads to the Hanle effect. In this paper, I discuss the physics of Hanle effect, and its influences on the backward scattering intensity of Na, K, and Fe atomic transitions and the associated Na and Fe resonant fluorescence lidar systems.

1. INTRODUCTION

It is well known that the dipole moment responsible for non-resonant Rayleigh scattering is coherently excited by a laser beam. In a resonant scattering process, the scattered photons are spontaneous emissions from atoms excited during the process. That such atoms, quite different from those involved in a fluorescence light, are also coherently excited is not as well known. Unlike incoherent excitation in the case of a fluorescence light, which leads to isotropic emission, the coherent excitation by a laser beam leads to angular distribution of emitted (or scattered) light, an antenna pattern if you wish. The difference between the two leads to the Hanle effect. We discuss the physics and formulation of the Hanle effect, and apply it to the backscattering of Na, K, and Fe atoms, and in turn treat the associated consequences on the associated resonance fluorescence lidar signals.

2. METHODOLOGY

A semiclassical/quantum mechanical treatment aimed at lidar applications was recently presented [1]. The resonant scattering cross-section from initial state $|f>$ via excited state $|F>$ to the final state $|f'>$ is given in (16) of the paper. By recognizing $\Gamma_{mm'} = A_{Ff'} / \left(2\alpha_{Ff'}\right)$, we have Eq. (1):

$$\frac{d\sigma^{RS}_{fFf'}}{d\Omega} = \frac{1}{4\pi}\frac{\lambda^2_{Ff}}{4}\frac{3}{2}\frac{g_F}{g_f}A_{Ff}\,g(\omega-\omega_{Ff})\,\alpha_{Ff'}C_{fFf'}(\hat{e};\hat{e}')$$

Here, $\lambda_{Ff}, g_F, g_f, A_{Ff}, \alpha_{Ff'}, and\ g(\omega-\omega_{Ff})$ are respectively, transition wavelength, excited state degeneracy, ground state degeneracy, Einstein A coefficient from excited to initial state, fractional transition rate, and absorption line-shape. The backscattering strength factor $C_{fFf'}(\hat{e};\hat{e}')$ is responsible for the angular distribution in question and it depends on the incident and scattering polarizations, $\hat{e}\ and\ \hat{e}'$. Referring to the basic scattering coordinate and geometry shown in Fig. 3 of She et al. [1], there are 4 cases denoting as: $C_{fFf'}(\hat{e}_a;\hat{e}_a')$, $C_{fFf'}(\hat{e}_a;\hat{e}_b')$, $C_{fFf'}(\hat{e}_b;\hat{e}_a')$, and $C_{fFf'}(\hat{e}_b;\hat{e}_a')$, each of which may be realized in laboratory experiments by the use of a polarizer and analyzer. However, for atmospheric applications, we consider only the cases where the radiated power of both $\hat{e}'_a$ and $\hat{e}'_b$ polarizations are received. Thus, we only evaluate $C_{fFf'}(\hat{e}_a;\hat{e}') \equiv C_{fFf'}(\hat{e}_a;\hat{e}'_a) + C_{fFf'}(\hat{e}_a;\hat{e}'_b)$ and $C_{fFf'}(\hat{e}_b;\hat{e}') \equiv C_{fFf'}(\hat{e}_b;\hat{e}'_a) + C_{fFf'}(\hat{e}_b;\hat{e}'_b)$ as given in (B8a) and (B8c) of [1]. To allow for the possibility of more than one emission final state, we define the differential cross section, summing all allowed emission pathways, with $\alpha_{Ff'} = A_{Ff'} / \sum_{f'} A_{Ff'}$, we have the desired differential cross-section as Eq.(2):

$$\frac{d\sigma^{RS}_{fF\Sigma}}{d\Omega} = \sum_{f'}\frac{d\sigma^{RS}_{fFf'}}{d\Omega} = \frac{1}{4\pi}\frac{\lambda^2_{Ff}}{4}\frac{3}{2}\frac{g_F}{g_f}A_{Ff}\,g(\omega-\omega_{Ff})\left[3\sum_{f'}\alpha_{Ff'}C_{fFf'}(\hat{e};\hat{e}')\right]$$

We denote the quantity in the square bracket as the distribution function of the fluorescence intensity, $I \equiv \left[3\sum_{f'}\alpha_{Ff'}C_{fFf'}(\hat{e};\hat{e}')\right]$. To make a complex discussion manageable, we simplify our discussion to a judiciously selected case with incident polarization as $\hat{e} = \hat{e}_b = -\hat{z}$, as in the textbook discussion of classical scattering, giving the fluorescence intensity as Eq. (3):

$$I \equiv \left[3\sum_{f'}\alpha_{Ff'}C_{fFf'}(\hat{e}_b;\hat{e}')\right] = \frac{2}{3}\left\{1+\frac{9}{2}\left(g_F\sum_{f'}\alpha_{Ff'}B^{(2)}_{fFf'}\right)\left[\frac{-2\left(2-3\sin^2\theta\right)}{30}\right]\right\}$$

Here the coefficient is given in terms of the 6-j coefficient in (16) of [1].

With the above simplification, we now consider two cases for pathedagogy reason and lidar application.

2.1 Physics demonstrated in a simple system

We now apply these formulae to the simplest quantum structure without spin-orbit or hyperfine interaction, and substitute $f = f' = 0$ and $F = 1$ into Eq. (3) the 6-j coefficients for $B^{(2)}_{fFf'}$. As a result, we obtain $g_1 = 3$, $\alpha_{10} = 1$ and $B^{(2)}_{101} = 5/9$, leading to the fluorescence intensity functions, $I = 3C_{010}(\widehat{-z};\hat{e}') = \sin^2\theta$, an angular distribution agreeing with the classical results in textbook [2]. This clearly demonstrated the difference from the spontaneous emission distribution that the Hanle effect is not of quantum origin. Rather, it is because of the excitation of the atomic system by a laser-like source, which coherently prepares the mixed excited sub-states before fluorescence emission. Indeed, the Hanle effect has a classical explanation and is most prominent when the excited sub-states are degenerate, i.e., when there is no Zeeman splitting at B = 0; thereby, it is an effective tool for measuring the lifetime of atomic excited states [3].

2.1 Hanle effect of Na, K and Fe transitions

In order to apply the formulation to atoms of practical interest, we need to evaluate this factor $g_F \sum_{f'} \alpha_{Ff'} B^{(2)}_{fFf'}$ for the transitions of Na, K, and Fe atoms. Though tedious, this can be down in a straightforward manner. The results for Na and K are given in Table 2.1.a and for Fe in Table 2.1.b below. Substitute these values into Eq. (2), we can calculate the fluorescence intensity distribution function $I(\theta)$ as well as that in the backward direction, $I(\theta) = \left[3\sum_{f'} \alpha_{Ff'} C^{\pi}_{fFf'}(-\hat{z};\hat{e}') \right]$ for realistic atoms for lidar application.

Table 2.1.a $g_F \sum_{f'} \alpha_{Ff'} B^{(2)}_{fFf'}$ for Na D_2 transitions

$g_F \sum_{f'} \alpha_{Ff'} B^{(2)}_{fFf'}$	F=3	F=2	F=1	F=0
$\left(2, \sum_{f'}\right)$	2/5	0	-1/15	
$\left(1, \sum_{f'}\right)$		0	1/3	0

Table 2.1.b $g_J \sum_{j'} \alpha_{Jj'} B^{(2)}_{jJj'}$ for Fe transitions

$g_J \sum_{j'} \alpha_{Jj'} B^{(2)}_{jJj'}$	$z^5F^0_4$	$z^5F^0_5$	$z^5D^0_4$
$a\,^2D_3, \left(\sum_{j'}\right)$	0.257		- 0.380
$\left(a\,^2D_4, \sum_{j'}\right)$	-0.400	0.289	0.532

Although the Hanle effect for Na D transitions in connection with lidar applications has been discussed in the literature, see for example Fricke and von Zahn [4] and Krueger et al. [5], its implications on Fe lidar considered [Höffner, private communication] but not yet evaluated. We present the radiation patterns for both for comparison here.

3. RESULTS

3.1 Radiation (antenna) patterns of laser induced fluorescence from Na and Fe atoms

Using the recipe presented for the simple case of z-polarized $\left(\hat{e} = -\hat{z}\right)$ incident beam, we compute and plot the radiation patterns for Na atom in Fig. 3.1.a and that for Fe atom in Fig. 3.1.b below.

The backward values, $\left[3\sum_{f'} \alpha_{Ff'} C^{\pi}_{fFf'}(-\hat{z};\hat{e}') \right]$, for Na excitations (2,1), (1,1) and (2,3), shown respectively in solid (blue, green and red) are 0.653, 0.733, and 0.747, corresponding to, respectively, 98%, 110% and 112% of its isotropic average. The backscattering values for Fe transitions at 386 nm (black), 372 nm (red), 374 nm (blue), 392 nm (light green) and 368 nm (dark green), respectively, are 1.160, 1.087, 1.077, 0.886 and 0.880 times their isotropic average of 2/3.

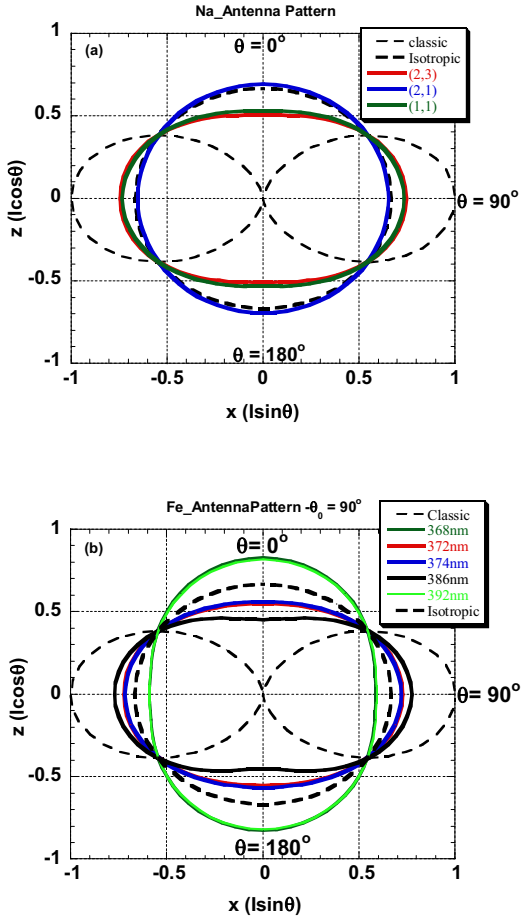

Fig. 3.1. Radiation patterns of the z-polarized, $\hat{e} = -\hat{z}$, dipole with fluorescence intensity $I = \left[3\sum_{f'} \alpha_{Ff'} C_{fFf'}(-\hat{z};\hat{e}') \right]$ as a function of scattering angles for (a) Na D_2 and (b) ^{56}Fe transitions. In (a), the Na (2,2), (1,2) and (1,0) excitations exhibit spontaneous emission behavior (bold-black dashed) with a backward scattering value of interest equal to the isotropic value, $3C^{\pi}_{fFf'}(-\hat{z};\hat{e}') = < 3C_{fFf'}(-\hat{z};\hat{e}') > = 2/3$. In (b), none of the Fe transitions exhibits spontaneous emission behavior (shown in bold-black dashed for reference). All transitions, shown in solid lines, exhibit the Hanle Effect. In both figures, for comparison the classic dipole pattern is shown in the thin-black dashed line.

3.2 Relevance to resonance fluorescence lidars

We consider the relevance of Hanle effect and apply the results outlined in Section 3.1 to Na and Fe fluorescence lidars. We do not discuss K lidar in part because its similarity with Na lidar and smaller atmospheric abundance. The simplest lidar (often broadband) for measuring metal density uses a transmitting laser beam. In this case, the Hanle effect could amount to up top 12 % density error. For atmospheric temperature and wind measurements, typically, intensity ratios are invoked. If the two or three frequencies in the ratio(s) are from the same atomic transition, as in the 3-frequency Na lidar [5], then the correction of the Hanle effect does not affect the temperature or wind retrieval. However, the accompanying Na density determination will still be affected. A different situation exists in the temperature determination with iron Boltzmann lidar, in which, the intensity ratio of 374 nm and 372 nm transitions is used. In this case, unless the multiplicative factors on the intensity of the two lines due to the Hanle effect are the same, they should be included. Fortunately, in this case, the multiplicative factors are nearly the same, respectively 1.077 and 1.087, ignoring the Hanle effect is justifiable.

We had only discussed the Hanle effect at B = 0. This is also justifiable, not only because the earth magnetic field is small compare to the internal magnetic field in the atom [5], also the Hanle effect is largest at B=0.

Note added in proof: A more extensive version of this paper has since been published [7].

REFERENCES

[1] C.-Y. She, H. Chen, and D. A. Krueger, "Optical Processes for middle atmospheric doppler lidars: cabannes scattering and laser-induced resonance fluorescence," *J. Opt. Soc. Am.* **B 32**, 1575–1592 (2015).

[2] D. J. Griffiths, *Introduction to Electrodynamics*, 2nd ed. (Prentice-Hall, 1981), p. 381.

[3] A. Corney, *Atomic and Laser Spectroscopy* (Oxford, 1977).

[4] K. H. Fricke and U. von Zahn, "Mesopause temperatures derived from probing the hyperfine structure of the D_2 resonance line of sodium by lidar", *J. Atmos. Terr. Phys*. **47**, 499–512 (1985).

[5] D. A. Krueger, C.-Y. She, and T. Yuan, "Retrieving mesopause temperature and line-of-sight wind from full-diurnal-cycle Na lidar observations," *Appl. Opt.*, **54**, 9469 – 9489 (2015).

[6] X. Chu, W. Pan, G. Papen, C. S. Gardner, and J. Gelbwachs, "Fe Boltzmann temperature lidar: Design, error analysis, and initial results at the North and South Poles", *Appl. Opt.*, **41**, 4400 – 4410 (2002).

[7] C.-Y. She, "Hanle effect in laser-induced fluorescence and Na and Fe resonance scattering lidars", **Appl. Opt., 58**, 8354 – 8361 (2019).